Detecting THz current fluctuations in a quantum point contact using a nanowire quantum dot

S. Gustavsson,* I. Shorubalko, R. Leturcq, T. Ihn, and K. Ensslin
Solid State Physics Laboratory, ETH Zurich, CH-8093 Zurich, Switzerland

S. Schön
FIRST Laboratory, ETH Zurich, CH-8093 Zurich, Switzerland

(Dated: May 9, 2008)

We use a nanowire quantum dot to probe high-frequency current fluctuations in a nearby quantum point contact. The fluctuations drive charge transitions in the quantum dot, which are measured in real-time with single-electron detection techniques. The quantum point contact (GaAs) and the quantum dot (InAs) are fabricated in different material systems, which indicates that the interactions are mediated by photons rather than phonons. The large energy scales of the nanowire quantum dot allow radiation detection in the long-wavelength infrared regime.

Charge detection with single-electron precision provides a highly-sensitive method for probing properties of mesoscopic structures. If the detector bandwidth is larger than the timescale of the tunneling electrons, single-electron transitions may be detected in real-time. This allows a wealth of experiments to be performed, like investigating single-spin dynamics [1], probing interactions between charge carriers in the system [2] or measuring extremely small currents [3, 4, 5]. The quantum point contact (QPC) is a convenient detector capable of resolving single electrons [6]. Recently, it has been shown that the QPC not only serves as a measurement device but also induces back-action on the measured system [7, 8, 9]. The concepts of detector and measured system can therefore be turned around, allowing a mesoscopic device like a quantum dot (QD) to be used to detect current fluctuations in the QPC at GHz frequencies [10].

In this work we investigate a system consisting of a QPC defined in a GaAs two-dimensional electron gas (2DEG) coupled to an InAs nanowire QD. We first show how to optimize the charge sensitivity when using the QPC as single-electron detector. Afterwards, the system is tuned to a configuration where electron tunneling is blocked due to Coulomb blockade. With increased QPC voltage bias we detect charge transitions in the QD driven by current fluctuations in the QPC. The fact that the QPC and the QD are fabricated in different material systems makes it unlikely that the interactions are mediated by phonons [8]. Instead, we attribute the charge transitions to absorption of photons emitted from the QPC [9, 10, 11].

Figure 1(a) shows a scanning electron microscope (SEM) image of the device used in these experiments. An InAs nanowire is deposited on top of a shallow (37 nm) AlGaAs/GaAs heterostructure based two-dimensional electron gas (2DEG). The QPC is defined by etched trenches, which separate the QPC from the rest of the 2DEG. The parts of the 2DEG marked by L and R are used as in-plane gates. The horizontal object in the figure is the nanowire lying on top of the surface, electrically isolated from the QPC. The QD in the nanowire and the QPC in the underlying 2DEG are defined in a single etching step using patterned electron beam resist as an etch mask. The technique ensures perfect alignment between the two devices. Details of the fabrication procedure can be found in Ref. 12. The electron population of the QD is tuned by applying voltages to the gates L and R. When changing gate voltages, we keep the QPC potential fixed by applying a compensation voltage V_{2DEG} to the 2DEG

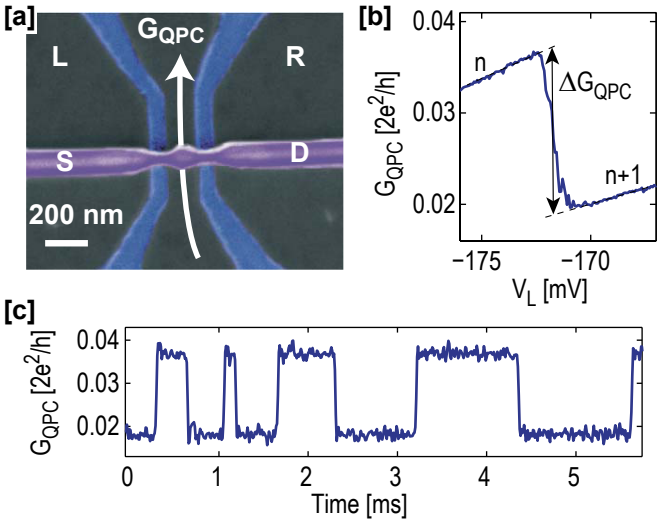

FIG. 1: (color online) (a) SEM image of the device. The quantum dot is formed in the nanowire, with the quantum point contact located in the 2DEG directly beneath the QD. (b) QPC conductance measured versus voltage on gate L. At $V_{\mathrm{L}} = -172\,\mathrm{mV}$ an electron is added to the QD, leading to a decrease of G_{QPC}. (c) Time trace of the QPC conductance measured at $V_{\mathrm{L}} = -172\,\mathrm{mV}$, showing a few electrons tunneling into and out of the QD. The upper level corresponds to a situation with n electrons on the QD.

*Electronic address: simongus@phys.ethz.ch

connected to both sides of the QPC. All measurements presented here were performed at an electron temperature of $T = 2$ K.

I. CHARGE DETECTION WITH A QUANTUM POINT CONTACT

Figure 1(b) shows a measurement of the QPC conductance as a function of voltage on gate L. The gate voltage tunes both the QPC transmission as well as the electron population on the QD. The measurement was performed without any bias voltage applied to the QD and with the drain lead of the QD pinched off. At $V_{\rm L} = -172\,{\rm mV}$, the electrochemical potential of the QD shifts below the Fermi levels of the source lead and an electron may tunnel onto the QD. This gives a decrease $\Delta G_{\rm QPC}$ of the QPC conductance corresponding to the change $\Delta q = {\rm e}$ of the charge population on the QD. The curve in Fig. 1(b) shows the average QPC conductance giving the time-averaged QD population. By performing a time-resolved measurement, electron tunneling can be detected in real-time. This is visualized in Fig. 1(c), where the measured QPC conductance fluctuates between the two levels corresponding to n and $n+1$ electrons on the QD. Transitions between the levels occur on a millisecond timescale, which provides a direct measurement of the tunnel coupling between the QD and the source lead [13]. By analyzing the time intervals between transitions, the rates for electrons tunneling into or out of the QD can be determined separately [14].

Next, we investigate the best regime for operating the QPC as a charge detector. The conductance of a QPC depends strongly on the confinement potential $U_{\rm QPC}(\vec{r})$. When operating the QPC in the region between pinch-off and the first plateau ($0 < G < 2e^2/h$), a small perturbation $\delta U_{\rm QPC}(\vec{r})$ leads to a large change in conductance δG. If a QD is placed in close vicinity to the QPC, we expect a fluctuation δq in the QD charge population to shift the QPC potential $U_{\rm QPC}(\vec{r})$ and thus give rise to a measurable change in QPC conductance. A figure of merit for using the QPC as a charge detector is then

$$\frac{\delta G}{\delta q} = \frac{\delta G\left[U_{\rm QPC}(\vec{r})\right]}{\delta U_{\rm QPC}(\vec{r})}\,\frac{\delta U_{\rm QPC}(\vec{r})}{\delta q}. \qquad (1)$$

The first factor describes how the conductance changes with confinement potential, which depends strongly on the operating point of the QPC. The second factor describes the electrostatic coupling between the QD and the QPC and is essentially a geometric property of the system.

The performance of the charge detector depends strongly on the operating point of the QPC. The best sensitivity for a device of given geometry is expected when the QPC is tuned to the steepest part of the conductance curve. This corresponds to maximizing the factor $\delta G/\delta U_{\rm QPC}$ in Eq. (1). In Fig. 2(a) we plot the conductance change ΔG for one electron entering the QD versus

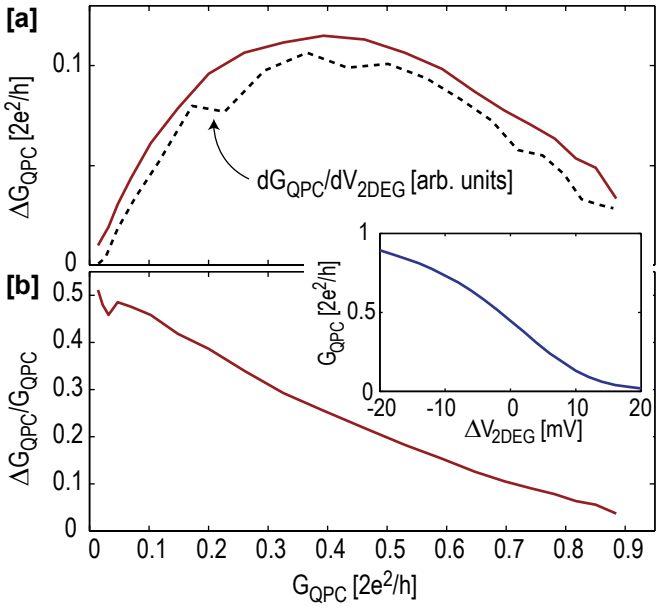

FIG. 2: (color online) (a) Change of QPC conductance as one electron enters the QD, measured for different values of average QPC conductance. The dashed line is the numerical derivative of the QPC conductance with respect to gate voltage. The change is maximal at $G_{\rm QPC} = 0.4 \times 2e^2/h$, which coincides with the steepest part of the QPC conductance curve [see inset in (b)]. (b) Relative change of QPC conductance for one electron entering the QD, defined as $(G_{\rm high} - G_{\rm low})/G_{\rm high}$. The relative change increases with decreased $G_{\rm QPC}$, reaching above 50% at $G_{\rm QPC} = 0.02 \times 2e^2/h$. The inset shows the variation of $G_{\rm QPC}$ as a function of gate voltage.

QPC conductance, in the range between pinch-off and the first conductance plateau ($0 < G_{\rm QPC} < 2e^2/h$). The change ΔG is maximal around $G_{\rm QPC} \sim 0.4 \times 2e^2/h$ but stays fairly constant over a range from 0.3 to $0.6 \times 2e^2/h$. The dashed line in Fig. 2(a) shows the numerical derivative of $G_{\rm QPC}$ with respect to gate voltage. The maximal value of ΔG coincides well with the steepest part of the QPC conductance curve. The inset in the figure shows how the conductance changes as a function of gate voltage.

In Fig. 2(b), we plot the relative change in conductance $\Delta G/G_{\rm QPC}$ for the same set of data. The relative change increases monotonically with decreasing conductance, reaching above 50% at $G_{\rm QPC} = 0.02 \times 2e^2/h$. The relative change in QPC conductance $\Delta G_{\rm QPC}/G_{\rm QPC}$ in this particular device is extraordinarily large compared to top-gate defined structures, where $\Delta G_{\rm QPC}/G_{\rm QPC}$ is typically around one percent for the addition of one electron on the QD [15, 16]. We attribute the large sensitivity to the close distance between the QD and QPC ($\sim$50 nm, due to the vertical arrangement of the QD and QPC) and to the absence of metallic gates on the heterostructure surface, which reduces screening.

The results of Fig. 2 indicate that it may be preferable to operate the charge detector close to pinch-off, where

the relative change in conductance is maximized. The quantity relevant for optimal detector performance in the experiment is the signal-to-noise (S/N) ratio between the change in conductance ΔG and the noise level of the QPC conductance measurement. We measure the conductance by applying a fixed bias voltage $V_{\rm SD}$ across the QPC and monitoring the current. In the linear response regime, both the average current $I_{\rm QPC}$ and the change in current for one electron on the QD ($\Delta I_{\rm QPC}$) scale linearly with applied bias. The noise in the setup is dominated by the voltage noise of the amplifier, which is essentially independent of the QPC operating point and the applied bias in the region of voltages discussed here. The S/N thus scale directly with $\Delta I_{\rm QPC}$

$$S/N = \frac{\Delta I_{\rm QPC}^2}{\langle \Delta I_{\rm noise}^2 \rangle} \propto V_{\rm QPC}^2 \, \Delta G^2 = I_{\rm QPC}^2 \left(\frac{\Delta G}{G} \right)^2 . \quad (2)$$

In practice the maximal usable QPC current is limited by effects like heating or emission of radiation which can influence the measured system. If we consider limiting the current, we see from Eq. (2) that the highest S/N is reached for the maximal value of $\Delta G/G$ at $G_{\rm QPC} \ll 2e^2/h$. However, this operation point requires a large voltage bias to be applied to the QPC. If the QPC bias is larger than the single-particle level spacing of the QD, the current in the QPC may drive transitions in the QD and thus exert a back-action on the measured device [9] (see next section). Therefore, a better approach is to limit the QPC voltage. Here, the best S/N is obtained when optimizing ΔG rather than $\Delta G/G$ and operating the QPC close to $G_{\rm QPC} = 0.5 \times 2e^2/h$. The sensitivity of the QPC together with the bandwidth of the measurement circuit allows a detection time of around 4 μs [5]. The tunneling rates presented in the following were extracted taking the finite detector time into account [17].

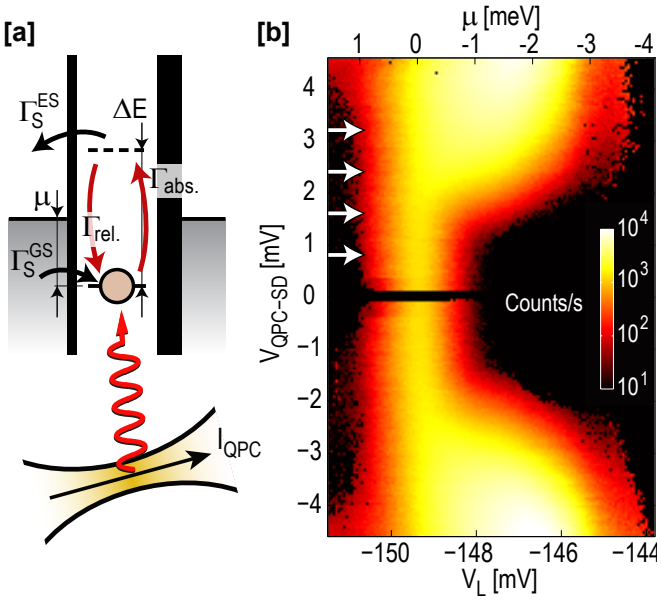

FIG. 3: (a) Energy level diagram describing the absorption process. The electron in the QD is excited due to photon absorption, which allows it to tunnel out to the lead. (b) Quantum dot excitations, measured versus QPC bias voltage. The main peak at $\mu = 0$ is due to equilibrium fluctuations between the source lead and the QD. As the gate voltage $V_{\rm L}$ is increased, the electrochemical potential of the QD drops below the Fermi level of the lead and only tunneling processes involving QD excitations become possible. Photon absorption is only possible for QPC bias voltages higher than the QD level separation ΔE, giving rise to the shoulder-like features appearing at high $V_{\rm QPC}$. The data was extracted from QPC conductances traces taken at $G_{\rm QPC} = 0.4 \times 2e^2/h$, filtered at 50 kHz. The data taken at low QPC bias $|V_{\rm QPC}| < 0.4$ mV was filtered at a lower bandwidth (15 kHz) to allow counting in this regime.

II. EXCITATIONS DRIVEN BY THE QUANTUM POINT CONTACT

In this section we study QD transitions driven by current fluctuations in the QPC. Such excitations were already studied for QDs and QPCs defined in a GaAs 2DEG [7, 8, 9]. From those experiments, it was not clear how energy was mediated between the systems. The nanowire sample investigated here is conceptionally different because the QD and the QPC are fabricated in different material systems. This allows us to make a statement about the physical processes involved in transmitting energy between the QD and the QPC. Since the two structures sit in separate crystals with different lattice constants and given that the systems hardly touch each other, we can assume that phonons only play a minor role as a coupling mechanism. Instead, we assume the QD transitions to be driven by radiation emitted from the QPC [10]. Another advantage of the nanowire structure compared to GaAs systems is that the QD energy scales are an order of magnitude larger compared to QDs formed in a GaAs 2DEG. This allows us to investigate radiation at several 100 GHz, reaching into the long-wavelength infrared regime.

We first discuss the QD configuration used for probing the radiation of the QPC. Since the QD level spectrum is not tunable, we can only drive transitions at fixed frequencies corresponding to excited states in the QD [7]. Figure 3(a) shows the level configuration of the system, with the QD electrochemical potential μ below the Fermi level of the leads. The tunneling barriers are highly asymmetric, with the barrier connecting the QD to the drain lead being almost completely pinched off. We do not apply any bias voltage to the QD. The system is in Coulomb blockade, but by absorbing a photon the QD may be put into an excited state with electrochemical potential above the Fermi energy of the leads. From here, the electron may leave to the source contact, the QD is refilled and the cycle may be repeated.

In Fig. 3(b) we plot the electron count rate versus QD potential and QPC bias. The peak at $\mu = 0$ is due to equilibrium fluctuations between the QD and the source

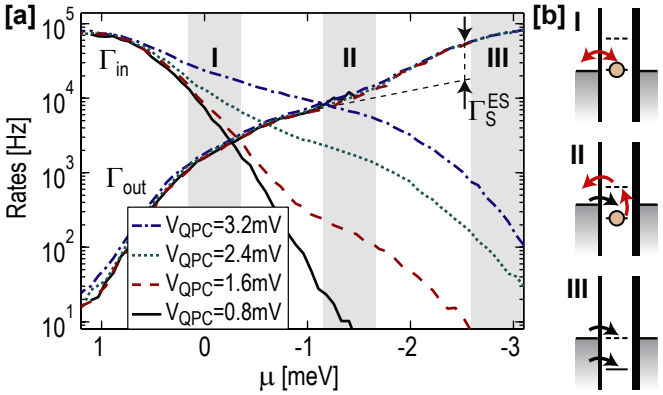

FIG. 4: (a) Rates for electrons tunneling into and out of the QD, measured at four cross-sections of Fig. 3(b) [position of arrows in Fig. 3(b)]. Only the rate related to absorption ($\Gamma_{\rm out}$) is strongly influenced by the increase in QPC bias. (b) Energy level diagrams for the three configurations marked in (a).

contact, with the width set by the electron temperature in the lead. As the QPC bias is increased above $\approx 2.5\,\mathrm{mV}$, a shoulder appears in the region of $\mu < 0$. This is consistent with the picture in Fig. 3(a); we need to apply a QPC bias larger than the single-level spacing for the photon-assisted tunneling to become possible. The width of the shoulder is set by $\Delta E \approx 2.5\,\mathrm{meV}$ and is therefore expected to be independent of QPC bias; we will see later in this section that the apparent smearing of the features in Fig. 3(b) are due to temperature and tuning of the tunneling rates. The picture is symmetric with respect to $V_{\rm QPC}$, meaning that the emission and absorption processes do not depend on the direction of the QPC current. The lack of data points around $V_{\rm QPC} = 0$ are due to the fact that the low QPC bias prevents the operation of the QPC as a charge detector. Due to the asymmetric coupling of the QD to the source and drain lead, we could not make a direct confirmation of the existence of an excited state with $\Delta E = 2.5\,\mathrm{mV}$ using finite bias spectroscopy. However, the value is consistent with excited states found in Coulomb diamond measurements in regimes where the tunnel barriers are more symmetric [5].

Figure 4(a) shows the separate rates for electrons tunneling into and out of the QD at horizontal cross-sections of Fig. 3(b), measured at four different QPC bias voltages [marked by arrows in Fig. 3(b)]. Around the resonance [$\mu = 0$, case I in Fig. 4], the tunneling is due to equilibrium fluctuations and the rates for tunneling into and out of the QD are roughly equal. By lowering the electrochemical potential μ the rate for electrons leaving the QD first falls off exponentially due to the thermal distribution of the electrons in the lead. Continuing to case II of Fig. 4, we come into the regime of QD excitations. Here, the rate $\Gamma_{\rm out}$ is directly related to the absorption process sketched in Fig. 3(a), while the rate $\Gamma_{\rm in}$ corresponds to the refilling of an electron from the lead. Consequently, $\Gamma_{\rm out}$ shows a strong QPC bias dependence, while $\Gamma_{\rm in}$ stays roughly constant.

In case III, the excited state goes below the Fermi level of the source lead and the absorption rate drops quickly. At the same time, $\Gamma_{\rm in}$ increases as the refilling of an electron into the QD may occur through either the ground state or the excited state. This provides a way to determine the tunnel coupling between the source contact and the excited state in the QD ($\Gamma_{\rm S}^{\rm ES}$). From the data in Fig. 4(a), we estimate $\Gamma_{\rm S}^{\rm ES} \approx 60\,\mathrm{kHz} - 20\,\mathrm{kHz} = 40\,\mathrm{kHz}$. The change of tunnel coupling with gate voltage makes the exact determination of $\Gamma_{\rm S}^{\rm ES}$ difficult, the value given here should only be considered as a rough estimate.

The tunneling rates within the region of photon-assisted tunneling are strongly depending on gate voltage. Similar effects have been investigated in 2DEG QDs, where the tunneling rate of a barrier was shown to depend exponentially on gate voltage due to tuning of the effective barrier height [18]. A difference of our sample compared to 2DEG QDs concerns the properties of the electronic states in the leads. For GaAs QDs, the leads consist of a two-dimensional electron gas where the ideal density of states (DOS) is independent of energy. For the nanowire QD, the leads are also parts of the nanowire and the corresponding electron DOS may show strong variations with energy due to the quasi-one dimensionality and finite length of the wire. Within the region of photon-assisted tunneling in Fig. 4(a), we shift the electrochemical potential of the QD and thereby change the energy of the tunneling electrons relative to the Fermi level in the lead. The measured tunneling rates could therefore show variations due to changes in the DOS in the lead.

However, the behavior seen in region II of Fig. 4(a) is not compatible with the effects discussed in the previous paragraph. The rate $\Gamma_{\rm in}$ is directly related to the tunnel coupling $\Gamma_{\rm S}^{\rm GS}$ between the source lead and the QD ground state, while the rate $\Gamma_{\rm out}$ depends on the coupling $\Gamma_{\rm S}^{\rm ES}$ between source and the excited state in the QD. For arguments based on barrier tuning and varying electron DOS, we would expect both $\Gamma_{\rm S}^{\rm GS}$ and $\Gamma_{\rm S}^{\rm ES}$ to change in the same way with gate voltage. This is in disagreement with the results of Fig. 4(a); $\Gamma_{\rm in}$ *increases* while $\Gamma_{\rm out}$ *decreases* with gate voltage. Instead, we speculate that the observed behavior may be due to non-resonant processes involving energy relaxation in the leads. Focusing on the energy level configuration pictured in Fig. 3(a), we see that there are a large number of occupied states in the lead with energy higher than the electrochemical potential of the QD. Elastic tunneling into the QD can only occur for electrons with energy equal to the electrochemical potential of the QD, but electrons at higher energy may contribute to the measured rate in terms of processes involving relaxation. As we lower μ, the number of initial states available for the inelastic processes increase and would therefore explain the *increase* in $\Gamma_{\rm in}$ with decreased μ. Inelastic tunneling is also possible for electrons leaving the QD excited state to empty states in

the lead. Here, the number of empty states available for the inelastic processes goes down when the QD potential is lowered. This is in agreement with the measured *decrease* in $\Gamma_{\rm out}$ with decreased μ.

III. QPC BIAS DEPENDENCE

Next, we investigate how the QPC bias influences the efficiency of the photon absorption process. For this purpose we apply a rate-equation model similar to that used for investigating QPC-driven excitations in double QDs [9]. The model consists of three states, corresponding to the QD being empty, populated with an electron in the ground state, or populated with an electron in the excited state. We write down the master equation for the occupation probabilities $p = [p_{\rm GS},\ p_{\rm ES},\ p_0]$ of the three states

$$\frac{d}{dt}\begin{bmatrix} p_{\rm GS} \\ p_{\rm ES} \\ p_0 \end{bmatrix} = \begin{bmatrix} -\Gamma_{\rm abs} & \Gamma_{\rm rel} & \Gamma_{\rm S}^{\rm GS} \\ \Gamma_{\rm abs} & -(\Gamma_{\rm S}^{\rm ES}+\Gamma_{\rm rel}) & 0 \\ 0 & \Gamma_{\rm S}^{\rm ES} & -\Gamma_{\rm S}^{\rm GS} \end{bmatrix} \begin{bmatrix} p_{\rm GS} \\ p_{\rm ES} \\ p_0 \end{bmatrix}. \tag{3}$$

Here, $\Gamma_{\rm abs}$ is the absorption rate and $\Gamma_{\rm rel}$ is the relaxation rate of the QD. The rates are visualized in Fig. 3(a). The charge detection technique can only probe rates for electrons entering or leaving the QD. These rates are found from the steady-state solution of Eq. (3):

$$\begin{aligned} \Gamma_{\rm in} &= \Gamma_{\rm S}^{\rm GS}, \\ \Gamma_{\rm out} &= \Gamma_{\rm S}^{\rm ES}\frac{p_{\rm ES}}{p_{\rm ES}+p_{\rm GS}} = \Gamma_{\rm S}^{\rm ES}\frac{\Gamma_{\rm abs}}{\Gamma_{\rm S}^{\rm ES}+\Gamma_{\rm abs}+\Gamma_{\rm rel}}. \end{aligned} \tag{4}$$

In GaAs QDs, the charge relaxation process occurs on a timescale of ~ 10 ns [19]. Similar rates are expected for nanowire QDs. Therefore, we assume $\Gamma_{\rm S}^{\rm ES} \ll \Gamma_{\rm rel}$ and estimate the behavior of $\Gamma_{\rm out}$ in the limit of weak absorption ($\Gamma_{\rm abs} \ll \Gamma_{\rm rel}$). Here, Eq. (4) simplifies to

$$\Gamma_{\rm out} = \Gamma_{\rm S}^{\rm ES}\,\Gamma_{\rm abs}/\Gamma_{\rm rel}. \tag{5}$$

Under these conditions the measured rate $\Gamma_{\rm out}$ is expected to scale linearly with the absorption rate. Assuming the excitations to be driven by fluctuations in the QPC current, we can combine Eq. (5) with the QPC emission spectrum $S_I(\omega)$ [10],

$$\begin{aligned} \Gamma_{\rm out} &\propto \Gamma_{\rm S}^{\rm ES}\,S_I(\Delta E/\hbar) = \\ &= \Gamma_{\rm S}^{\rm ES}\,\frac{4e^2}{h}D(1-D)\frac{eV_{\rm QPC}-\Delta E}{1-e^{-(eV_{\rm QPC}-\Delta E)/k_BT}}, \end{aligned} \tag{6}$$

where D is the QPC transmission coefficient and T the electron temperature in the QPC leads. Note that Eq. (6) only gives the proportionality between $\Gamma_{\rm out}$ and $S_I(\omega)$; to make quantitative predictions for the absorption rate one needs to determine the overlap between the ground and the excited state. For a double QD, this coupling can be extracted from charge localization measurements [20]. However, it is not as straightforward to estimate the overlap for single-QD excitations. One would need to know the shape of the wavefunctions for the different QD states, which is not known.

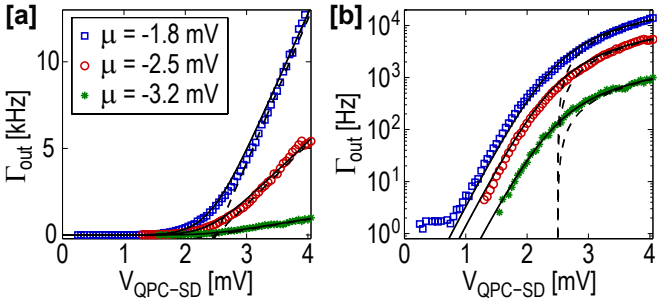

FIG. 5: (a) Electron tunneling due to photon absorption, measured versus QPC bias voltage. The data was taken at three different positions of the shoulder seen in Fig. 3. As soon as the QPC bias voltage exceeds the QD level separation ΔE, the absorption rate increases linearly with $V_{\rm QPC}$. (b) Same data as in (a), but plotted in logarithmic scale. The absorption rate shows exponential decay for $eV_{\rm QPC} < \Delta E$, with the slope of the decay set by the electron temperature in the QPC. The solid lines are fits to Eq. (6) in the text, while the dashed lines are the corresponding results assuming zero temperature.

In Fig. 5 we plot the measured tunneling rate $\Gamma_{\rm out}$ related to absorption versus bias on the QPC, measured for three different electrochemical potentials of the QD. The traces correspond to vertical cross-sections for positive $V_{\rm QPC}$ in Fig. 3(b). Figure 5(a) shows the rates plotted on a linear scale; the rates taken at all three positions increase linearly with QPC bias as soon as $eV_{\rm QPC} > \Delta E$. The solid lines are fits to Eq. (6) with $T = 2\,$K and assuming $\Delta E = 2.5\,$meV to be the same for all three traces. As described in the previous section, we attribute the difference in slope for the three cases to changes in effective tunnel coupling with gate voltage [see Fig. 4(a)]. Figure 5(b) shows the same data plotted on a logarithmic scale. Here, we see a clear exponential decay for $eV_{\rm QPC} < \Delta E$; this is due to the thermal distribution of electrons in the QPC [11]. The dashed lines in Fig. 5 show the rates expected for the case of zero temperature. The weak but non-zero count rate occurring at low QPC bias voltages ($V_{\rm QPC} < 1\,$mV) for the data taken at $\mu = -1.8\,\mu$eV is due to non-photon induced thermal fluctuations between the QD ground state and the lead.

To quantify the efficiency of the absorption process we compare the rates $\Gamma_{\rm out}$ and $\Gamma_{\rm S}^{\rm ES}$ using Eq. (5). Due to the strong change of $\Gamma_{\rm S}^{\rm ES}$ with gate voltage, we can only make a quantitative comparison between $\Gamma_{\rm out}$ and $\Gamma_{\rm S}^{\rm ES}$ in the region where we are able to determine $\Gamma_{\rm S}^{\rm ES}$ (around $-\mu = \Delta E$). This corresponds to the circles in Fig. 5. For this data set, the measured rate goes up to around 5 kHz for $V_{\rm QPC} = 4\,$mV, so that we still have $\Gamma_{\rm out} \ll \Gamma_{\rm S}^{\rm ES}$. This confirms that we are in a regime of weak absorption where the relative population of the excited state is much smaller than the population of the ground state. Note

that the same is most likely true also for the data sets taken at $\mu = -1.8\,\mathrm{mV}$ and $\mu = -3.2\,\mathrm{mV}$ in Fig. 5; however, we can not make a quantitative comparison with Γ_S^{ES} since we do not have an independent measurement of Γ_S^{ES} for those regions.

IV. CHANGING THE QPC OPERATING POINT

In this section, we modify the operating point of the QPC to check how this influences properties of the emitted radiation. Since we use the same QPC both for emitting radiation and for performing charge detection, it is not possible to operate the device at the plateaus where the conductance is fully quantized. However, we could tune the QPC conductance in a region between $0.05 \times 2e^2/h < G_{\mathrm{QPC}} < 0.8 \times 2e^2/h$ while still being able to detect the tunneling electrons.

In Fig. 6(a) we plot the electron count rate at the photon-absorption shoulder versus change in $V_{2\mathrm{DEG}}$. Figure 6(b) shows how the QPC conductance changes with gate voltage within the region of interest. Compensation voltages were applied to the gates L and R in order to keep the QD potential fixed while sweeping $V_{2\mathrm{DEG}}$. The data was taken with fixed $V_{\mathrm{QPC}} = 2\,\mathrm{mV}$ to make the photon absorption process possible. This bias is still lower than the characteristic sub-band spacing of the QPC, which is around 5 meV. The strong peak at the top of Fig. 6(a) ($\mu = 0$) corresponds to equilibrium fluctuations between the QD and the source lead. In the region of photon-assisted tunneling [marked by the arrow in Fig. 6(a)], the shoulder appears with increasing QPC conductance. Going above $G_{\mathrm{QPC}} = 0.5 \times 2e^2/h$, the strength of tunneling at the position of the shoulder decays slightly.

Assuming that the shoulder appears because of radiation emitted from shot noise fluctuations in the QPC current, we expect the measured absorption rate to depend on the transmission of the QPC. From Eq. (6) we see that the emission spectrum scales with $D(1-D)$, where D is the transmission coefficient of the channel. In Fig. 6(c) we plot the rate Γ_{out} related to the absorption process, measured at $\mu = -1.9\,\mathrm{meV}$ [position of the arrow Fig. 6(a)]. The dashed line shows the emission expected from the QPC, $S_I \propto D(1-D)$. For low G_{QPC}, the measured rate follows the expected emission spectrum reasonably well, with a maximum around $G_{\mathrm{QPC}} \approx 0.5 \times 2e^2/h$.

Still, the measured curve shows deviations compared to the predicted behavior. Suppression of noise close to $G_{\mathrm{QPC}} = 0.7 \times 2e^2/h$ has been reported [21, 22] to be related to 0.7 anomaly [23]. There are indications of the 0.7 anomaly also in our sample, but we believe the deviations in the measured noise spectrum are more likely to originate from an increase in background charge fluctuations triggered by the QPC current. At large QPC currents ($I_{\mathrm{QPC}} > 20\,\mathrm{nA}$), the noise in the system increases with I_{QPC}. This can not be attributed to the intrinsic QPC

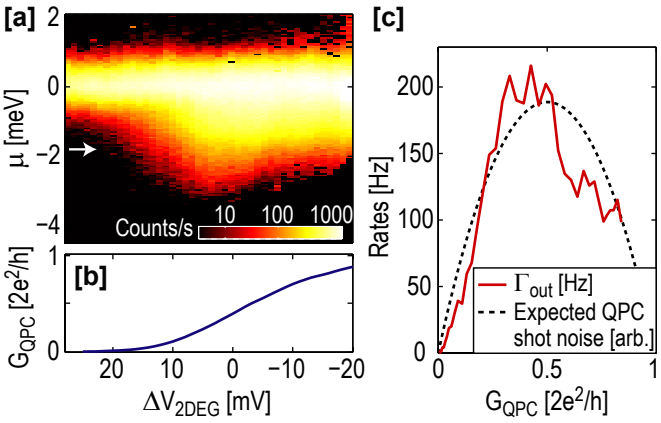

FIG. 6: (a) Electron count rate in the regime of the absorption process, measured versus gate voltage on the 2DEG. This corresponds to tuning the conductance of the QPC. A vertical cross-section corresponds to the shoulder seen in Fig. 3. The data was taken with $V_{\mathrm{QPC}} = 2\,\mathrm{mV}$. (b) QPC conductance as a function of gate voltage, measured for the same region as in (a). (c) Tunneling rate Γ_{out} associated with the absorption process, measured at $\mu = -1.8\,\mathrm{meV}$ [marked by an arrow in (a)]. The dashed line shows the expected emission spectrum of the QPC, up to a scaling factor depending on the efficiency of the absorption process.

shot noise but is rather due to fluctuations of trapped charges driven by the high QPC current. The QD is thus placed in an environment of fluctuating potentials, which may lead to QD transitions. The strength of such transitions depends strongly on the number of fluctuators in the neighborhood of the QD [24]. The charge traps also influence the count rate in the regime of tunneling due to equilibrium fluctuations [peak at $\mu = 0$ in Fig. 6(a)]. For $G_{\mathrm{QPC}} = 0.8 \times 2e^2/h$ ($\Delta V_{2\mathrm{DEG}} = -20\,\mathrm{mV}$), the peak is considerably wider than for $G_{\mathrm{QPC}} = 0.05 \times 2e^2/h$. Again, this can be attributed to a fluctuating potential at the location of the QD.

To minimize the influence of the charge traps, one would prefer to decrease V_{QPC} and operate the QPC at lower current levels. For the configuration used in Fig. 6 ($V_{\mathrm{QPC}} = 2\,\mathrm{mV}$), the QPC current reaches values above 100 nA at $G_{\mathrm{QPC}} \approx 0.7 \times 2e^2/h$. However, V_{QPC} can not be made too small; we need to make sure that eV_{QPC} is on the same order of magnitude as the level spacing ΔE, otherwise the QPC will not emit radiation in the right frequency range. The above discussion only concerns a measurement of the emission properties of the QPC. When using the device to probe radiation of an external source, the QPC can be operated at much lower bias voltages.

To summarize, we have used time-resolved charge detection techniques to investigate the influence of current flow in a near-by QPC to the electron population in nanowire QD. Since the QD and the QPC are fabricated in different material systems, we conclude that phonons can only play a minor role for a transferring energy between the structures. Instead, we attribute

the charge to absorption of photons emitted from the quantum point contact. The large energy scales of the nanowire QD allows detection of radiation at a frequency of $f = 2.5\,\mathrm{meV}/h = 0.6$ THz, thus reaching into the long-wavelength infrared regime. This is an order of magnitude larger than energy scales reachable with GaAs QDs [9].

[1] J. M. Elzerman, R. Hanson, L. H. Willems van Beveren, B. Witkamp, L. M. K. Vandersypen, and L. P. Kouwenhoven, Nature **430**, 431 (2004).

[2] S. Gustavsson, R. Leturcq, B. Simovic, R. Schleser, T. Ihn, P. Studerus, K. Ensslin, D. C. Driscoll, and A. C. Gossard, Phys. Rev. Lett. **96**, 076605 (2006).

[3] J. Bylander, T. Duty, and P. Delsing, Nature **434**, 361 (2005).

[4] T. Fujisawa, T. Hayashi, R. Tomita, and Y. Hirayama, Science **312**, 1634 (2006).

[5] S. Gustavsson, I. Shorubalko, R. Leturcq, S. Schön, and K. Ensslin, Appl. Phys. Lett. **92**, 152101 (2008).

[6] M. Field, C. G. Smith, M. Pepper, D. A. Ritchie, J. E. F. Frost, G. A. C. Jones, and D. G. Hasko, Phys. Rev. Lett. **70**, 1311 (1993).

[7] E. Onac, F. Balestro, L. H. W. van Beveren, U. Hartmann, Y. V. Nazarov, and L. P. Kouwenhoven, Phys. Rev. Lett. **96**, 176601 (2006).

[8] V. S. Khrapai, S. Ludwig, J. P. Kotthaus, H. P. Tranitz, and W. Wegscheider, Phys. Rev. Lett. **97**, 176803 (2006).

[9] S. Gustavsson, M. Studer, R. Leturcq, T. Ihn, K. Ensslin, D. C. Driscoll, and A. C. Gossard, Phys. Rev. Lett. **99**, 206804 (2007).

[10] R. Aguado and L. P. Kouwenhoven, Phys. Rev. Lett. **84**, 001986 (2000).

[11] E. Zakka-Bajjani, J. Ségala, F. Portier, P. Roche, D. C. Glattli, A. Cavanna, and Y. Jin, Phys. Rev. Lett. **99**, 236803 (2007).

[12] I. Shorubalko, R. Leturcq, A. Pfund, D. Tyndall, R. Krischek, S. Schön, and K. Ensslin, Nano Letters **8**, 382 (2008).

[13] R. Schleser, E. Ruh, T. Ihn, K. Ensslin, D. C. Driscoll, and A. C. Gossard, Appl. Phys. Lett. **85**, 2005 (2004).

[14] S. Gustavsson, R. Leturcq, B. Simovic, R. Schleser, P. Studerus, T. Ihn, K. Ensslin, D. C. Driscoll, and A. C. Gossard, Phys. Rev. B **74**, 195305 (2006).

[15] L. M. K. Vandersypen, J. M. Elzerman, R. N. Schouten, L. H. Willems van Beveren, R. Hanson, and L. P. Kouwenhoven, Appl. Phys. Lett. **85**, 4394 (2004).

[16] D. J. Reilly, C. M. Marcus, M. P. Hanson, and A. C. Gossard, Appl. Phys. Lett. **91**, 162101 (2007).

[17] O. Naaman and J. Aumentado, Phys. Rev. Lett. **96**, 100201 (2006).

[18] K. MacLean, S. Amasha, I. P. Radu, D. M. Zumbühl, M. A. Kastner, M. P. Hanson, and A. C. Gossard, Phys. Rev. Lett. **98**, 036802 (2007).

[19] T. Fujisawa, D. G. Austing, Y. Tokura, Y. Hirayama, and S. Tarucha, Nature **419**, 278 (2002).

[20] L. DiCarlo, H. J. Lynch, A. C. Johnson, L. I. Childress, K. Crockett, C. M. Marcus, M. P. Hanson, and A. C. Gossard, Phys. Rev. Lett. **92**, 226801 (2004).

[21] P. Roche, J. Ségala, D. C. Glattli, J. T. Nicholls, M. Pepper, A. C. Graham, K. J. Thomas, M. Y. Simmons, and D. A. Ritchie, Phys. Rev. Lett. **93**, 116602 (2004).

[22] L. DiCarlo, Y. Zhang, D. T. McClure, D. J. Reilly, C. M. Marcus, L. N. Pfeiffer, and K. W. West, Phys. Rev. Lett. **97**, 036810 (2006).

[23] K. J. Thomas, J. T. Nicholls, M. Y. Simmons, M. Pepper, D. R. Mace, and D. A. Ritchie, Phys. Rev. Lett. **77**, 135 (1996).

[24] A. Pioda, S. Kičin, D. Brunner, T. Ihn, M. Sigrist, K. Ensslin, M. Reinwald, and W. Wegscheider, Phys. Rev. B **75**, 045433 (2007).